



Cite this: *Phys. Chem. Chem. Phys.*,
2016, 18, 29395

A Grotthuss-like proton shuttle in the anomalous $C_2H_3^+$ carbocation: energetic and vibrational properties for isotopologues†

Junjie Li, Alexander B. Pacheco, Krishnan Raghavachari and Srinivasan S. Iyengar*

We probe the structure, stability and vibrational properties of the fundamental $C_2H_3^+$ carbocation that exists with preference in a bridged hydrogen conformation. Our computational study includes electronic structure treatment, incorporation of nuclear motion through classical and quantum paradigms, the effect of temperature, and the associated sampling of the potential surface, and the effect of single H/D isotopic substitution (*i.e.*, $C_2H_2D^+$). We find that while the non-classical, "Bridged" isomer is most stable, the "Classical" form does have a small presence under ambient conditions since the zero point level straddles the barrier between the Classical and Bridged isomers in a reduced dimensional analysis of the Bridged \leftrightarrow Classical transfer coordinate. But the probability of the classical structure is too low and hence may remain undetected from the vibrational properties of the system. For the deuterated counterpart, the deuterium preferentially occupies the terminal instead of bridge position, in the more stable bridged isomeric structure. This preference is noted from nuclear dynamics. In all cases, at higher temperatures, an orbiting phenomenon is observed where the hydrogen atom density is distributed as an oblate ellipsoid surrounding the carbon–carbon bond. This is not observed at lower temperatures and the orbiting phenomenon is probed here by computing two-dimensional, time–frequency vibrational spectra, which show the spectral evolution in time and temperature, and the development of the system from one kind of isomer to another. New experiments that may probe this isomeric multiplicity are suggested, and these involve a combination of infra-red multiple photon dissociation (IRMPD) and argon-tagged action spectroscopy.

Received 24th June 2016,
Accepted 6th September 2016

DOI: 10.1039/c6cp04450f

www.rsc.org/pccp

1 Introduction

Carbocations are intermediates in organic reactions,^{1,2} common fragments in mass spectrometry,³ and have a large presence in extra-terrestrial gas clouds.^{4,5} Among the many carbocations of interest, $C_2H_3^+$ is one of the simplest, and yet controversial ions. This ion has two widely accepted stable structures that are both local minima on most known levels of electronic structure theory.⁶ One isomeric form is the vinyl cation ($HC^+=CH_2$), also referred to as the "Classical" structure (Fig. 1(a)), and has a "Y-shape"; the other has a proton positioned on top of the π -cloud between the two carbon atoms, forming a symmetric bridge structure and is commonly known as the protonated acetylene cation ($H^+(C_2H_2)$), or simply the "Bridged" isomer (Fig. 1(b)). As noted in Fig. 1, there are two distinct positions for the hydrogen nuclei in both cases. The Bridged isomer has one bridge and two terminal locations for hydrogen, whereas the

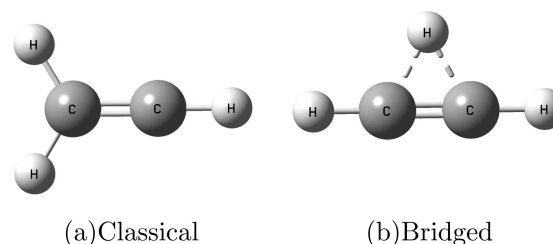


Fig. 1 The two well-known stable structures for $C_2H_3^+$: (a) the Classical vinyl cation and (b) the Bridged protonated acetylene cation. Nomenclature used to depict the various locations in this publication: (a) "Classical" isomer: CH_2 protons on the left and the CH proton on the right. (b) "Bridged" isomer: bridge proton in the middle and terminal protons on the side.

two terminal locations for Classical isomer are themselves distinct and may be referred to as CH and CH_2 locations.

There have been several experimental efforts to probe these stable structures. Early infrared spectroscopy studies^{7,8} indicate the Bridged form to be more stable, and these are consistent with more recent gas-phase, argon-tagged infrared action spectroscopy experiments.^{9,10} However, Coulomb explosion imaging

Department of Chemistry and Department of Physics, Indiana University,
800 E. Kirkwood Ave, Bloomington, IN-47405, USA. E-mail: iyengar@indiana.edu
† Electronic supplementary information (ESI) available. See DOI: 10.1039/c6cp04450f

experiments^{11,12} in conjunction with Car–Parrinello dynamics calculations^{13,14} indicate the possible sampling of non-planar configurations, with one proton primarily localized at the bridge position with the other two performing localized conical excursions about the carbon–carbon bond axis.

Theoretical efforts have mostly focused on electronic structure treatment, with a few exceptions where the effect of nuclei has been included within classical^{13,14} and quantum¹⁵ descriptions. For pure electronic structure treatment, Hartree–Fock calculations^{16–18} favor the Classical structure, but almost all electron correlation methods^{6,16–20} predict the Bridged structure to be more stable. This conclusion is further supported by vibrational self-consistent field and vibrational CI studies^{15,21} conducted using potential surfaces constructed at the CCSD(T) level of theory where the basis set contributions are extrapolated to the one-particle basis limit. Furthermore the potential surface in ref. 21 also includes core-correlation and scalar-relativistic corrections. The consensus of modern electronic structure calculations⁶ is that the Bridged structure is lower in energy by approximately 3.7–4.8 kcal mol⁻¹, and the transition state is 0.1–0.4 kcal mol⁻¹ above the Classical structure. The barrier height derived from the tunneling splitting in IR spectra^{7,22} is 4.25 kcal mol⁻¹ above the Bridged structure. Further details can be found in ref. 6 and 10.

While it appears from the above discussion that the problem is well understood, there are several questions that remain: the experiments do not probe the Classical structure and apart from the Coulomb explosion imaging,^{11,12} supported by Car–Parrinello dynamics simulations,¹⁴ the non-planar structure has not been seen. In addition, isotope-dependent vibrational CI and perturbation theory studies have been limited to the bridge conformation in ref. 21. While most infra-red spectra calculations that support the experimental findings of a bridge proton use a purely harmonic approximation with electronic structure, in ref. 21, the authors show that the bridge proton motion is facilitated by a highly anharmonic potential surface that appears to be quartic at the very least. Clearly, harmonic calculations do not describe the problem in sufficient detail, yet they appear to qualitatively describe the experimental findings.^{9,10}

Can deuteron substitution and the effect of internal temperature be used as a probe toward the structural promiscuity of this system? In ref. 23 and 24, it has been shown that for highly anharmonic systems that are characterized by a shared proton, deuterium substitution provides a qualitatively different set of vibrational features that can be rationalized through non-trivial coupling of the intrinsic harmonic modes. Furthermore, the temperature dependent behavior of such coupling was quite illuminating in deciphering the experimental situation.²⁴ In fact, the harmonic mode couplings in these highly anharmonic systems that lead to the final observed results^{23,24} are quite similar to those found²⁵ for the well known Zundel cation.^{25–27} As a result, in this publication, we undertake an exhaustive study of the problem that includes multiple electronic structure levels, and temperature dependent *ab initio* molecular dynamics studies for the Bridged and Classical protonated and deuterated isotopologues. In addition we have also considered approximations of the bridge hydrogen nucleus as a quantum nuclear

wavepacket. Our analysis tools include dynamically averaged vibrational spectral computations performed beyond the harmonic approximation, two-dimensional time–frequency spectral evolution of the vibrational density of states that probes the dynamics of the problem, along with several structural tools.

The paper is organized as follows: Section II shows the rationale behind the choice of electronic structure method used in the dynamics studies. The studies in Section II include benchmarks that encompass multiple levels of electronic theory. Section SI (ESI†) provides details on the *ab initio* molecular dynamics simulations constructed using the chosen electronic structure methods. Section III includes a discussion on the structural transformations (Classical ↔ Bridged) that occur during dynamics. Section III also includes an analysis of the bridge proton potential surface and associated quantum nuclear effects using techniques presented in Appendix A. In Section IV the vibrational properties are gauged including the evolution of the vibrational spectra as a function of time and temperature, which provide an additional handle on the structural transformation. Facilitating discussions on techniques used in Section IV are provided in Appendix B. Comparisons are made with vibrational spectra obtained from harmonic approximation and Classical ↔ Bridged inter-conversions are analyzed in terms of fluctuating populations in a selected set of harmonic modes. Section V includes a detailed structural and spectroscopic discussion on the singly deuterated isotopologue. Here again time–frequency analysis is used to probe structural transitions as a function of time and temperature. Section V(A) provides the likely experimental implications of our study. Conclusions are given in Section VI.

II. Choice of electronic structure theory

Table 1 provides a brief summary of the relative stability of the Bridged and Classical isomers and the height of the intervening barrier. The data provided include calculations performed here as well as those from previous studies.^{6,13,21} Clearly, the barrier and difference in energy between the Classical and Bridged isomers are dependent on the level of theory. Commonly used DFT functionals such as B3LYP, BLYP and PBE drastically underestimate the stability of the Bridged isomer; in fact, BLYP/6-311+G(3df,2pd) and B3LYP/6-31+G* provide trends that are inconsistent with other theories. On the other hand, MP2 significantly overestimates the stability of the Bridged isomer and here the Classical isomer is a transition state. Higher level electron correlation methods such as CCSD(T) and MRCI are all within 1 kcal mol⁻¹ in their prediction of the Bridged isomer stability. Given that our goals are to compute long term *ab initio* dynamics trajectories that include all levels of anharmonicity, and subsequently probe the quantum nuclear effects, our choice of electronic structure theory is based on both accuracy and efficiency. For example, the total AIMD simulation time for these systems, as discussed in the next sections, is of the order of 1 nanosecond (see ESI† for simulation details) and is used to

Table 1 Relative energies for the Bridged and Classical structures

Level of theory	$E_{\text{Classical}} - E_{\text{Bridged}}$ (kcal mol ⁻¹)	$E_{\text{TS}} - E_{\text{Classical}}^a$ (kcal mol ⁻¹)
M06-2X/6-311+G(3df,2pd)	4.45	0.21
CCSD(T)/cc-pVQZ ^b	3.66 ^c	0.07 ^c
CCSD(T)/6-311+G(3df,2pd) ^b	3.74 ^c	0.077 ^c
CCSD(T)/CBS ^d	3.94	
MRCI ^e	4.15	0.66 ^f
MRCI+Q ^g	4.02	
MP2/6-311+G(3df,2pd)	8.75	0.0 ^h
MP4/cc-pVQZ ^b	5.38 ^c	—
MP4/6-311+G(3df,2pd) ^b	5.43 ^c	—
LDA/35 Rydberg ⁱ	3.6	—
B3LYP/6-311+G(3df,2pd)	0.29	1.10
B3LYP/6-31+G*	-2.61	1.54
BLYP/6-311+G(3df,2pd)	-0.52	1.34
PBE/6-311+G(3df,2pd)	2.16	0.33

^a Transition state is calculated at the same level of theory as that for optimization, unless otherwise mentioned. ^b From Table 1 in ref. 6, which also includes a large number of other calculations that are all not reported here. See ref. 6 for further details. ^c Using CCSD/6-311+G(3pf,2pd) optimized geometries. ^d Ref. 21: includes core-correlation correction and a scalar-relativistic correction. ^e [5s 4p 2d 1f 3s 2p] ANO basis set with CASSCF/DZP optimized geometry, ref. 28. ^f Maximum along the CPF/TZ2P reaction path. ^g [6s 5p 3d 2f 4s 3p 2d] ANO basis set with CPF/TZ2P optimized geometry, ref. 29. ^h The classical structure is a transition state under this theory. ⁱ From ref. 13.

sample a wide range of the system potential surface. Given an average time step of the order of 0.25 fs, to help conserve the overall system Hamiltonian, this amounts to roughly a million electronic structure calculations which is clearly prohibitive even for this small a system when coupled cluster accuracy at the large basis limit is desired. [This situation is likely to change in the near future with the advent of new methods, such as the fragment based *ab initio* molecular dynamics method,^{30,31} that do provide MP2 and coupled cluster accuracy at much reduced computational cost.] As a result of these restrictions, we employ dynamical simulations constructed using the M06-2X³² functional with the 6-311+G(3df,2pd) Gaussian basis set for our analysis in this paper. The M06-2X functional favors the Bridged isomer by 4.45 kcal mol⁻¹ which is close to the energy difference from MRCI⁶ and from CCSD(T),²¹ and the transition state is 4.66 kcal mol⁻¹ above the Bridged structure (0.21 kcal mol⁻¹ above the Classical structure), well within the 4–5 kcal mol⁻¹ range of other theoretical⁶ and experimental estimates.^{7,8,22} Details regarding the *ab initio* molecular dynamics simulations constructed in this publication can be found in Section SI (ESI†). In total, 36 different simulations were constructed spanning a wide range of temperatures, for two different isotopologues. The total simulation time is roughly 1 nanosecond and is used to sample a wide range of the system potential surface. As such, the computed spectra are a direct function of the subspace of the global potential surface that is sampled at a given temperature. As a result temperature dependent properties are also constructed in our studies. In this regard the choice of temperature range in Section SI (ESI†) is particularly important to clarify. This choice determines the distribution of initial kinetic energy and the corresponding phase-space structural distribution function. Based on previous

AIMD studies on a wide range of hydrogen bonded systems, it is known that the argon-tagged action spectra are recorded using low temperature ions and AIMD trajectories in the 100 K range are in good agreement with these results.^{24,25,33–35} Similarly, computed trajectories above 390 K are generally in agreement with IRMPD experiments^{23–25,35} and these are what we consider to be higher temperatures below. As a result, the potential energy surface is sampled preferentially in these trajectories with temperatures chosen in the 50–600 K range. (The temperature is computed assuming equipartition theorem where the total kinetic energy is $\frac{3}{2}(N-1)kT$. This leads to an average kinetic energy for these simulations in the range 0.7–7 kcal mol⁻¹ as noted in ESI.†)

III. Structural properties from dynamics simulations: classical and quantum distributions

In many of our higher temperature simulations, the structure of C₂H₃⁺ is highly fluxional and the protons orbit the two carbon atoms. This phenomenon is portrayed in Fig. 2(a) and an animation depicting this process is shown in ESI.† In Fig. 2(a) we also note a situation that is reminiscent of the “Grothuss proton shuttle mechanism”³⁶ that has been widely invoked for the study of proton transport in water and other excess proton systems such as in polymer electrolyte membranes,³⁷ proton-conduction channels in biological enzymes and ion-channel systems.³⁸ In Fig. 2(b) we show the “Grothuss proton shuttle mechanism”³⁶ in a water-wire³⁹ for comparison purposes. The “Grothuss proton shuttle mechanism” is a cascading sequence of proton transfer events between strategically placed donor and acceptor groups. The process is similar to the treatment of valence electrons during the process of resonance in organic chemistry and happens during long-range proton transfer in water, in proton-conduction channels in biological enzymes and ion-channel systems and also in polymer-electrolyte membrane fuel cells. In the current situation, the strategically placed donor and acceptor groups for proton transfer belong to the carbon skeleton and do not yield long distance proton transfer, but do lead to a proton shuttle, that orbits the carbon skeleton. Hence we have termed this a Grothuss-like shuttle mechanism, since it shares many of the basic features of the parent process. In Fig. 2(c) we present the distribution of all three surrounding hydrogen nuclei around the central carbon atoms for such trajectories, where the dynamical, delocalized, nature of the protons is clearly noted. The distribution of the protons encapsulates the two carbon atoms at higher temperatures.

The fact that such hopping events are well-sampled during our classical trajectories is also seen from Fig. 3(a). Here a reduced dimensional distribution function (computed from dynamics trajectories) is shown on a plane defined by the two carbon atoms and the bridge proton. The color key in this plot represents the reduced probability of finding the system at the

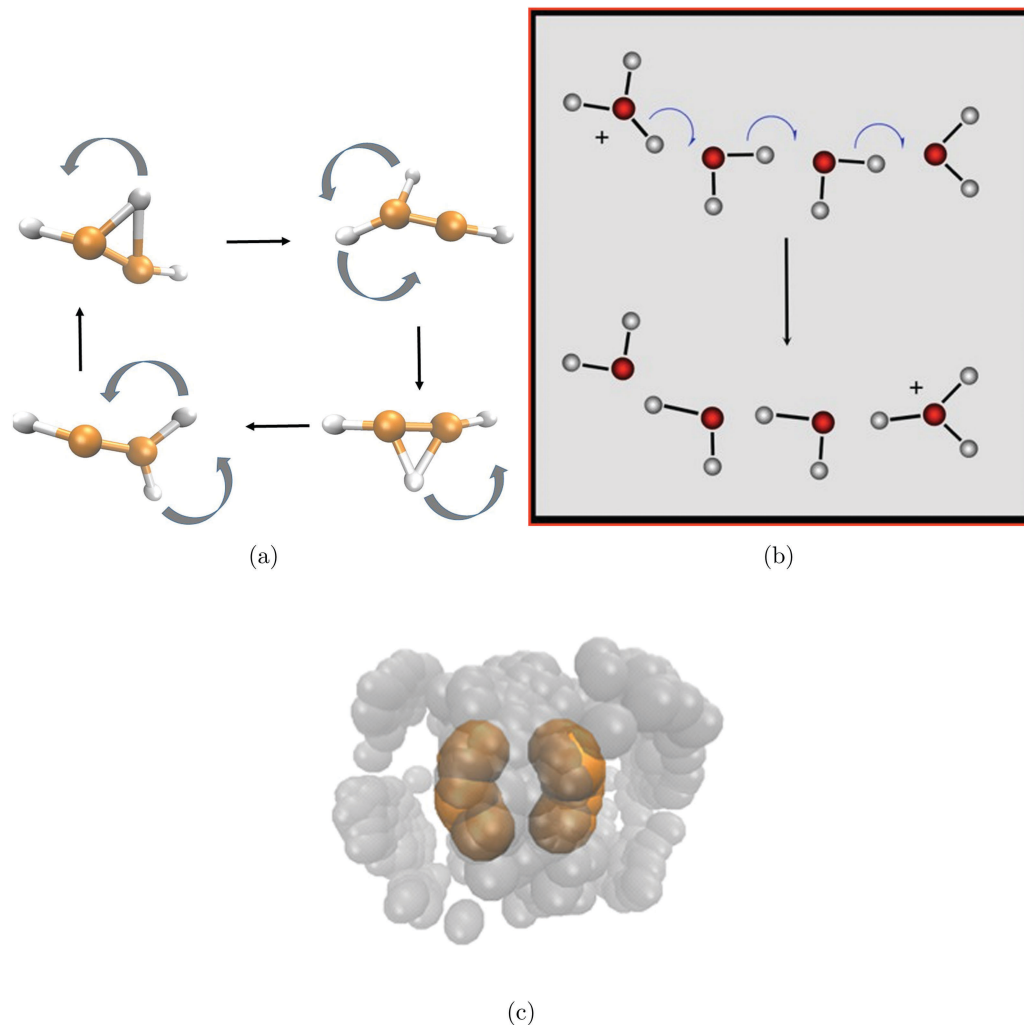


Fig. 2 (a) The fluxional nature of the $C_2H_3^+$ bridge proton for the high temperature calculations that is animated in ESI†. The hopping mechanism here is reminiscent of the “Grothuss proton shuttle mechanism”³⁶ that has been widely invoked for the study of proton transfer in water. This is shown in (b). (c) The distribution of all three hydrogen nuclei (gray) surrounding the central carbons (shown in orange). Panel (c) is also animated in ESI† to provide a clearer three-dimensional picture of the hydrogen nuclear distribution. The distribution has not been symmetrized. As can be seen from Table in SI (ESI†), all trajectories conserve the total energy of the system to within a few-tenths of a $kcal\ mol^{-1}$.

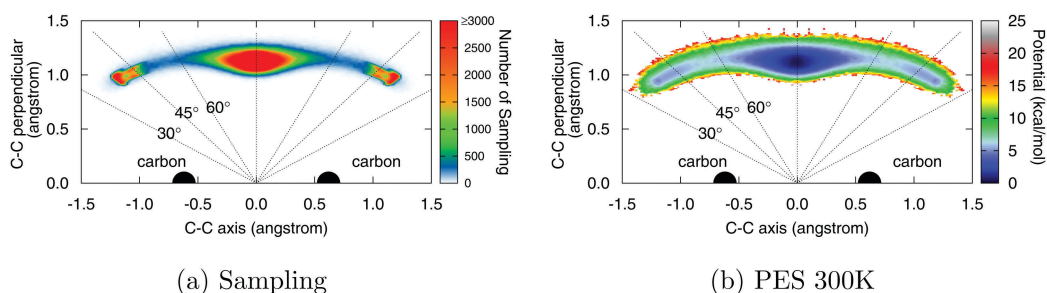


Fig. 3 (a) The sampling of the classical (between 30 and 45 degrees) and bridge (at 90 degrees) structures during our dynamics calculations. The sampling count is computed inside two dimensional bins where each bin has a size of 0.14 Å along the C–C axis and 0.07 Å in the noted orthogonal direction. The corresponding potential surfaces are shown in (b). The effect of temperature is as follows: since these plots are reduced dimensional, the orthogonal degrees of freedom that are sampled during dynamics need to be weighted to obtain an average value on these plots. The weighting function is Boltzmann, at 300 K. The Bridged structure, the Classical structure and the intervening barrier are clearly seen.

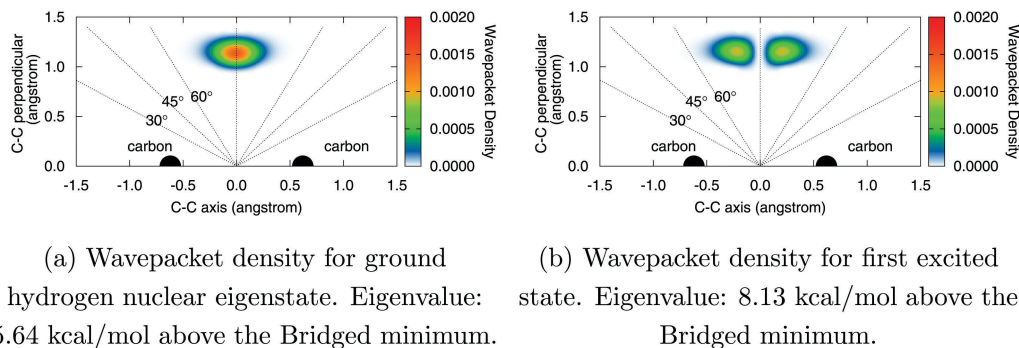


Fig. 4 The ground (a) and first excited (b) eigenstates corresponding to the potential in Fig. 3(b). The corresponding eigenvalues are 5.64 kcal mol⁻¹ above the Bridged minimum (a) and 8.13 kcal mol⁻¹ above the Bridged minimum (b). Despite the zero-point energy being over the barrier height, the ground and first excited states are mostly localized within the Bridged region of the potential. The corresponding deuterium eigenstates for the same potential are 4.02 kcal mol⁻¹ and 5.87 kcal mol⁻¹. That is the deuterium zero point energy is below the barrier.

given configuration. In a similar fashion, a reduced dimensional potential surface can also be constructed on the same plane where the orthogonal degrees of freedom are Boltzmann averaged at a chosen temperature, *i.e.*,

$$\frac{1}{Q} \int dq \delta(q - R_X) \exp[-\beta H] V(q) = \tilde{V}_\beta(R_X), \quad (1)$$

where R_X represents the two dimensional transfer coordinate shown in Fig. 3(a), the quantity “ q ” includes all degrees of freedom in the system and β is the inverse temperature, $\beta = 1/kT$. Thus the potential surface generated here is a thermally weighted “effective” surface for the bridge proton motion, which receives an average (thermalized) interaction from the motion of degrees of freedom orthogonal to R_X (denoted as R_X^\perp) and the associated

electronic structure change. It is clear from this potential that the thermalized barrier between the Bridged configuration (dark blue region in Fig. 3(b)) and the Classical configuration (light blue region at ≈ 45 degrees in Fig. 3(b)) is roughly 4.3 kcal mol⁻¹ and occurs at a little over 60 degrees.

Using the potentials in Fig. 3(b) that are thermally averaged along R_X^\perp , a proton Hamiltonian is then constructed in the position representation with the kinetic energy operator represented with “distributed approximating functionals” (DAFs)^{23,40-43} (see Appendix A). The corresponding nuclear Hamiltonian is then diagonalized using the Arnoldi iterative diagonalization procedure.^{44,45} The resultant eigenstate density for the first two states is shown in Fig. 4 and the respective eigenvalues are stated in the figure caption. *The zero point*

Table 2 Harmonic mode descriptions for C₂H₃⁺

	Bridged isomer			Classical isomer		
	Frequency (cm ⁻¹)	IR intensity ^a	Mode description	Frequency (cm ⁻¹)	IR intensity ^a	Mode description
Facilitator modes	668	26.22		1078	1.04	
	1271	6.00		183	38.61	
Inherent modes	690	0.00	Anti-symmetric CH bend _⊥ ^b	701	51.83	HCC out-of-plane bend
	789	114.08	Symmetric CH bend _⊥ ^a	858	102.41	CH wag _⊥ ^a
	920	50.03	CH bend _∥ ^c	1177	84.23	HCH bend _∥ ^b
	2000	9.81	HCCH symmetric stretch	1802	58.31	CC symmetric stretch
	2368	100.83	Bridge proton stretch	3012	299.80	CH ₂ symmetric stretch
	3242	424.74	CH symmetric stretch	3072	222.22	CH ₂ anti-symmetric stretch
	3358	0.00	CH anti-symmetric stretch	3306	126.99	CH stretch

^a In units of km mol⁻¹. ^b The “ \perp ” symbol implies motion perpendicular to the bridged hydrogen, carbon-carbon plane. ^c The “ \parallel ” symbol implies motion along the bridged hydrogen, carbon-carbon plane.

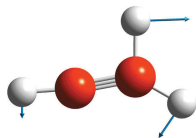


Fig. 5 The transition state normal mode with imaginary frequency (i 282 cm^{-1}) is qualitatively similar to the facilitator modes at 183 cm^{-1} for the Classical isomer and the 1271 cm^{-1} for the Bridged structure marked in Table 2.

energy is over the barrier that straddles the bridge and classical configurations. Despite this, the ground and excited state densities are strongly localized on the bridge configuration, as seen in Fig. 4. Furthermore, a straightforward fit of the potential in Fig. 3(b) is achieved only through a polynomial of order 12 along the curvilinear minimum energy coordinate, if both wells (Bridged and Classical) are to be reasonably represented. If only the Bridged conformer is to be represented, a 6th order polynomial would suffice, but as is clear this potential is highly anharmonic. While this result is partially consistent with that seen in ref. 21, where a quartic potential was found to be necessary to sample the Bridged isomer potential well alone, it is critical to note that the method used here samples the full anharmonicity of the potential, on all accessible minima. The configurational space is sampled based on the simulation temperature controlled by the classical nuclear kinetic energy. Furthermore, as will become clear in the next section, the

IV. Vibrational properties of C_2H_3^+ computed from dynamics

Before we embark on an analysis of the spectral intensities and frequencies obtained from dynamics, we first highlight the harmonic fundamentals since (a) the extent of fluxionality can be gauged as departure from spectral intensities predicted from harmonic approximation, and (b) using the harmonic spectrum we may identify “facilitator-modes” that closely identify with the Bridged \leftrightarrow Classical transition and “inherent modes” that characterize each isomer. Table 2 shows two facilitator modes that represent a reduced dimensional subspace within the molecular $3N$ dimensional space that appears to be directed along the Bridged \leftrightarrow Classical reaction path. Specifically, while the 668 cm^{-1} (Bridged) and 1078 cm^{-1} (Classical) modes show proton orbit directions, the 1271 cm^{-1} and 183 cm^{-1} modes represent modes that may encounter some resistance during the Bridged \leftrightarrow Classical transition.

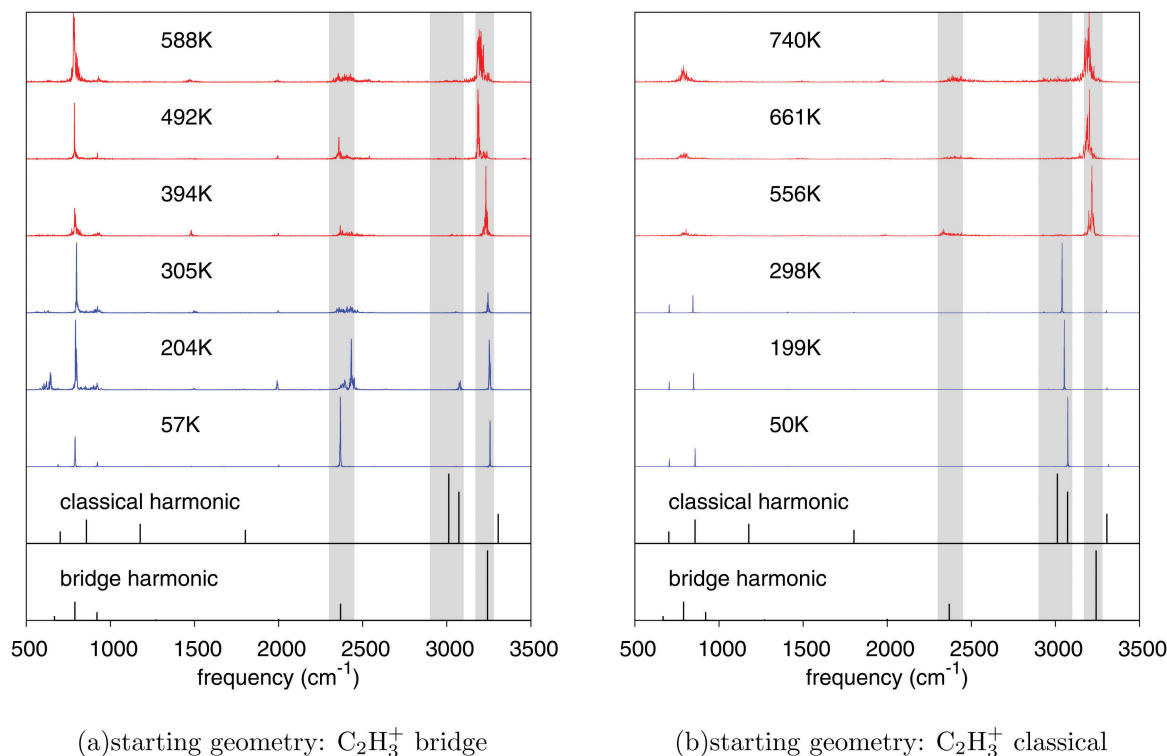


Fig. 6 IR spectra for C_2H_3^+ computed using $\alpha_\mu^{\text{OC}}(\omega)$ (eqn (B2)). In all cases the average simulation temperature is noted. The bottom two panels are harmonic spectra for the Bridged and Classical structures. The blue and red spectra are obtained from trajectories computed using (a) the Bridged structure $\text{H}^+(\text{CH}=\text{CH})$ as starting geometry and (b) the Classical structure $\text{HC}^+=\text{CH}_2$ as starting geometry. Trajectories containing conformational transitions between Bridged and Classical structures are shown in red.

Furthermore, the mode corresponding to the imaginary frequency for the transition state between the Bridged and Classical isomers (see Fig. 5) is similar to the 183 cm^{-1} mode for the Classical isomer and the 1271 cm^{-1} mode for the Bridged isomer.

While the harmonic approximation is a reasonable starting point for most rigid covalent systems, the fluxional system here displays a great deal of anharmonicity as noted in the previous section. Our previous results on such anharmonic systems^{23–25,33–35,50} indicate that the spectrum for such systems may be dominated by how the harmonic modes couple to produce new modes in the presence of anharmonicity. In a sense then, the temperature in a classical simulation acts as an additional handle that gradually tunes in anharmonicity by changing the extent to which the potential surface is sampled. For the current situation, we simulate the vibrational spectra by computing one-dimensional and two-dimensional Fourier transforms for the dipole–dipole auto-correlation function obtained from the dynamics trajectories. These expressions are presented in Appendix B, specifically see eqn (B2) and (B3). Furthermore, to understand spectral diffusion as it may materialize when the isomer populations change during dynamics, we also compute the two-dimensional Fourier transforms of the velocity–velocity auto-correlation function (eqn (B4)) which is related to the local kinetic energy as a function of time and frequency. In these approaches, the fully sampled region of the potential surface is involved and anharmonicity is included depending on the extent of sampling. Temperature is the single parameter that modulates this sampling and $\alpha_{\mu}^{\text{QC}}(\omega)$ in eqn (B2) has been shown to accurately reproduce vibrational properties in agreement with vibrational action spectroscopy experiments.^{23–25,33,34} Furthermore, these kinds of studies have also been used in the past to understand the differences between experimental techniques^{23,24} such as infra-red multiple photon dissociation (IRMPD)^{51–55} and argon tagged action spectroscopy,^{56,57} (This aspect is used later in Section V(A) where we discuss the implications of our results for experiment.) In fact, as far as we are aware, the studies in ref. 23 and 24 represent the first time that a high level of concordance has been achieved between the experiments, IRMPD^{51–53,58–61} and argon-tagged action spectroscopy,⁵⁶ and a single set of theoretical results, for a set of spectra of a hydrogen-bound system, incorporating both a wide temperature range and isotopic effects.

A selected set of vibrational spectra for C_2H_3^+ are shown in Fig. 6. The harmonic fundamentals are also presented as part of the bottom two panels in Fig. 6 with intensities stated in Table 2. For the lower average temperature spectra in blue, the $\alpha_{\mu}^{\text{QC}}(\omega)$ -spectra (eqn (B2)) share features with the harmonic results for the appropriate starting geometries. This is noted using the gray shading in Fig. 6 to guide the eye. For temperatures above 400 K, Classical \leftrightarrow Bridged isomer transformation begins and the spectra show a convergent behavior irrespective of the starting geometry. Importantly, when proton hops do occur, the respective spectra are dominated by the lower energy Bridged structure. Thus, the dominant presence of the Bridged spectral features in the vibrational spectra does not obviously imply that the Classical structure is not sampled during dynamics.

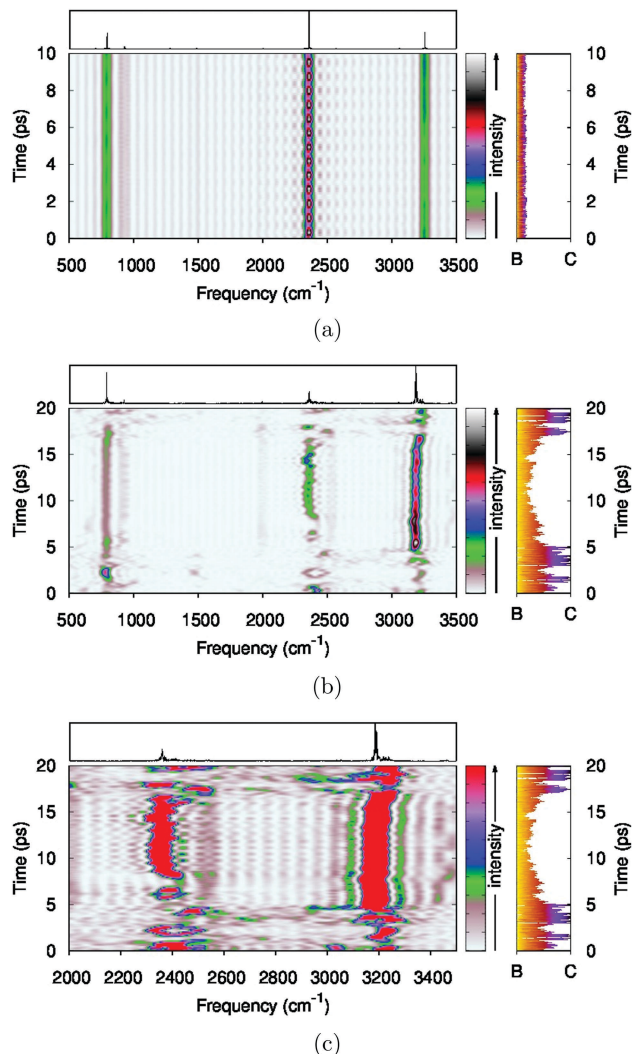


Fig. 7 Two-dimensional time–frequency analysis for C_2H_3^+ using $\alpha_{\mu}^{\text{QC}}(T, \omega; \Delta T)$ (eqn (B3)) conducted at (a) 107 K average temperature when no conformational transition occurs and (b) 492 K average temperature when the structure dynamically changes between Bridged and Classical configurations. Both trajectories use the Bridged structure as starting geometry. In (c) the spectrum in (b) is further focused to the most relevant region for conformational transition. The maximum peak height here is 1/10th the peak height at 3100 cm^{-1} to assist in viewing the lower intensity spectral transitions. In all figures, the spectra on the top are corresponding one dimensional $\alpha_{\mu}^{\text{QC}}(\omega)$ (eqn (B2)) spectra, and the plots on the right side are time evolution of a conformational transition parameter in Appendix C where the letter “B” is used to refer to the Bridged structure and “C” for the Classical structure.

For example, this is certainly not the case for the trajectories that begin with the classical structure in Fig. 6(b).

To understand the hopping process at higher temperatures, we compute the spectral evolution by considering two-dimensional time–frequency spectra in Fig. 7 and 8. Clearly, in Fig. 7(b) and (c), peaks do appear in the 3000 cm^{-1} region a few times during dynamics, and conversion between the two local minima generates nonzero intensity in the $3000\text{--}3100\text{ cm}^{-1}$ (Classical) spectral region. But those intensities are low compared to the intensity near the 3250 cm^{-1} peak corresponding to the Bridged isomer CH stretch, and hence can barely be seen in the overall spectrum. As a result,

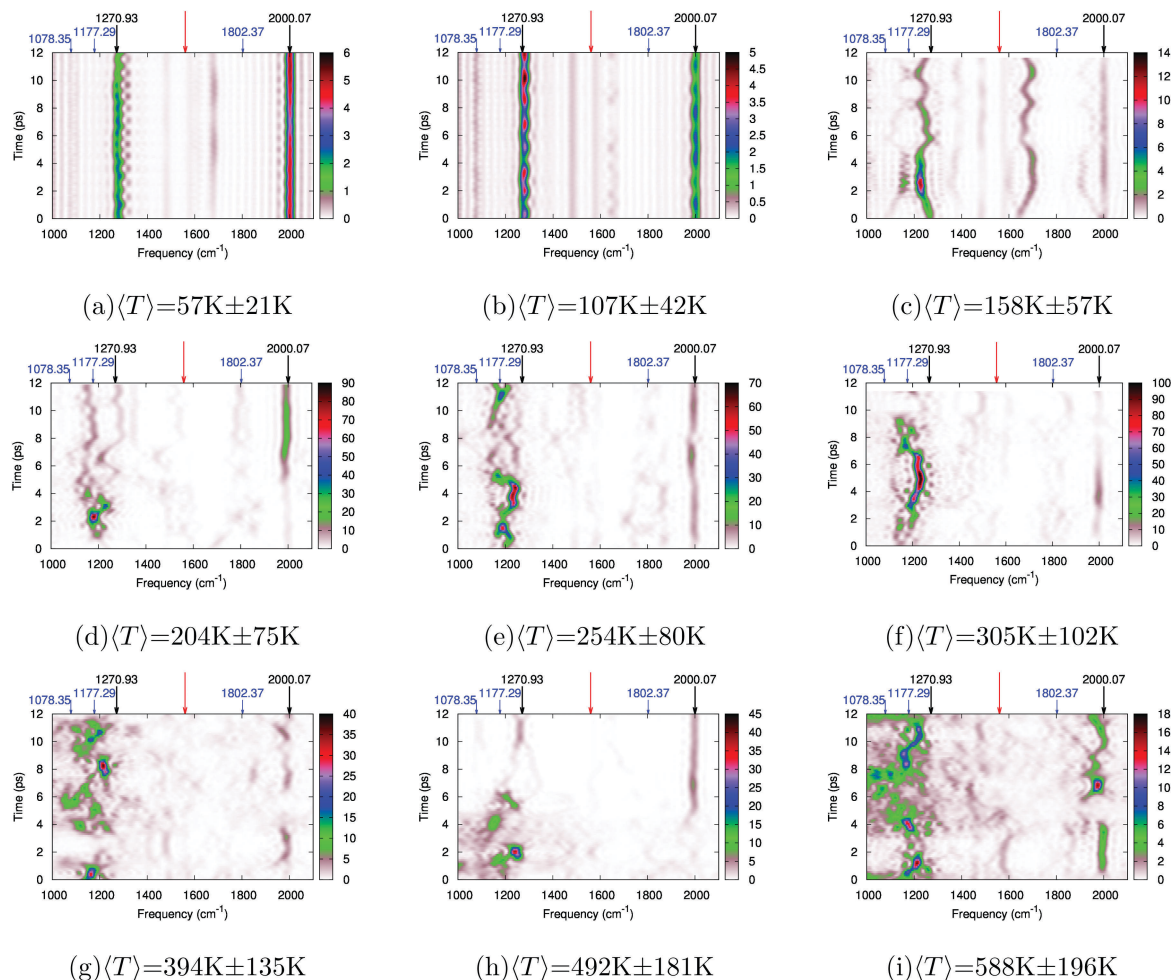


Fig. 8 The quantity $\alpha_{\nu}(T, \omega; \Delta T)$ in eqn (B4) is plotted in the time–frequency domain for multiple temperatures. To guide the eye, these figures are also provided as a single animation in the ESI.† The critical Bridged (black) and Classical (blue) modes that appear to participate in the Bridged \leftrightarrow Classical transition are noted on the top axis. See Table 2 for normal mode descriptions.

the vibrational spectra are dominated by features from the Bridged isomer, and dynamical conversion is not easily seen from the resulting spectrum.

In Fig. 8 we inspect the time–frequency velocity auto-correlation function shown in eqn (B4) for the spectral range 1000–2100 cm^{-1} . This spectral range is specifically chosen in the dark region for the Bridged isomer within the harmonic approximation (see bottom panels in Fig. 6 and Table 2). Upon inspection of the animation in Fig. 8, we note that at low temperatures, the 1271 cm^{-1} Bridged \leftrightarrow Classical facilitator mode and the 2000 cm^{-1} CC symmetric stretch mode (both dark modes) for the Bridged system are populated and a reasonable amount of kinetic energy exists in these normal-mode directions. (Note that the intensities in Fig. 8 are not spectral intensities, but are computed according to eqn (B4).) However, as the temperature is raised, one notes substantial contribution from the bright Classical HCH bend_{||} mode at 1177 cm^{-1} and the dark Classical facilitator mode at 1078 cm^{-1} . We also see some contribution from the dark classical CC symmetric stretch mode at 1802 cm^{-1} . Note further that the dark modes at 1271 cm^{-1} and 1078 cm^{-1} are Bridged \leftrightarrow Classical facilitator modes and hence any energy in these directions implies the existence of flux

in the Bridged \leftrightarrow Classical population transfer direction. For convenience, the specific set of modes that participate in this process are marked on top in Fig. 8.

V. Vibrational spectra and relative stability of the Bridged and Classical isomers in the single H/D substituted isotopologue

To further probe the dynamics seen in the previous section, we consider isotopic substitutions and break the symmetry of the problem. We replace one proton in C_2H_3^+ with a deuterium. Consequently, there are two different Bridged structures and two different Classical structures, and these are shown in Fig. 9. Based purely on electronic structure, there is no difference in stability between the two Classical and two Bridged forms.

Similar to the studies on C_2H_3^+ , the dynamical studies for $\text{C}_2\text{H}_2\text{D}^+$ are also performed over a wide range of temperatures.

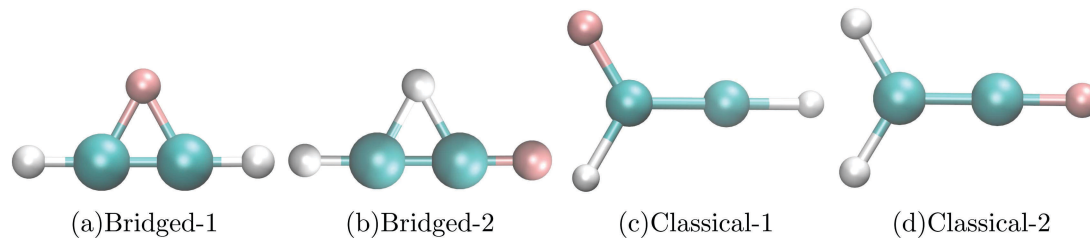


Fig. 9 Stable structures for singly deuterated $C_2H_2D^+$ optimized at M06-2X/6-311+G(3df,2pd). The deuterium is shown in magenta. The nomenclature used to depict the proton positions is stated in Fig. 1.

Two different starting geometries are chosen: the Bridged-1 and the Classical-1, and details regarding these simulations are shown in Table SI (ESI[†]). The dynamically computed $\alpha_{\mu}^{QC}(\omega)$ -spectra are shown in Fig. 10 and facilitator modes from the harmonic approximation are shown in Table 3. As in the case of $C_2H_3^+$, the energy along these facilitator mode directions should yield isomeric transitions. The complete set of harmonic spectra for the four isomeric forms are shown in the bottom panel of Fig. 10.

Again, at lower temperatures, the dynamical spectra closely resemble the harmonic results at the corresponding starting geometries. But when conformational transformations begin to occur, new peaks emerge in the vicinity of the 3291 cm^{-1} peak corresponding to the Bridged-1 harmonic spectrum and the 3308 cm^{-1} which coincides with the harmonic peak from the Bridged-2 configuration. Another spectroscopic signature that indicates the inter-conversion of structures is at about 2500 cm^{-1} , which coincides with a peak that only exists in Bridged-2 and

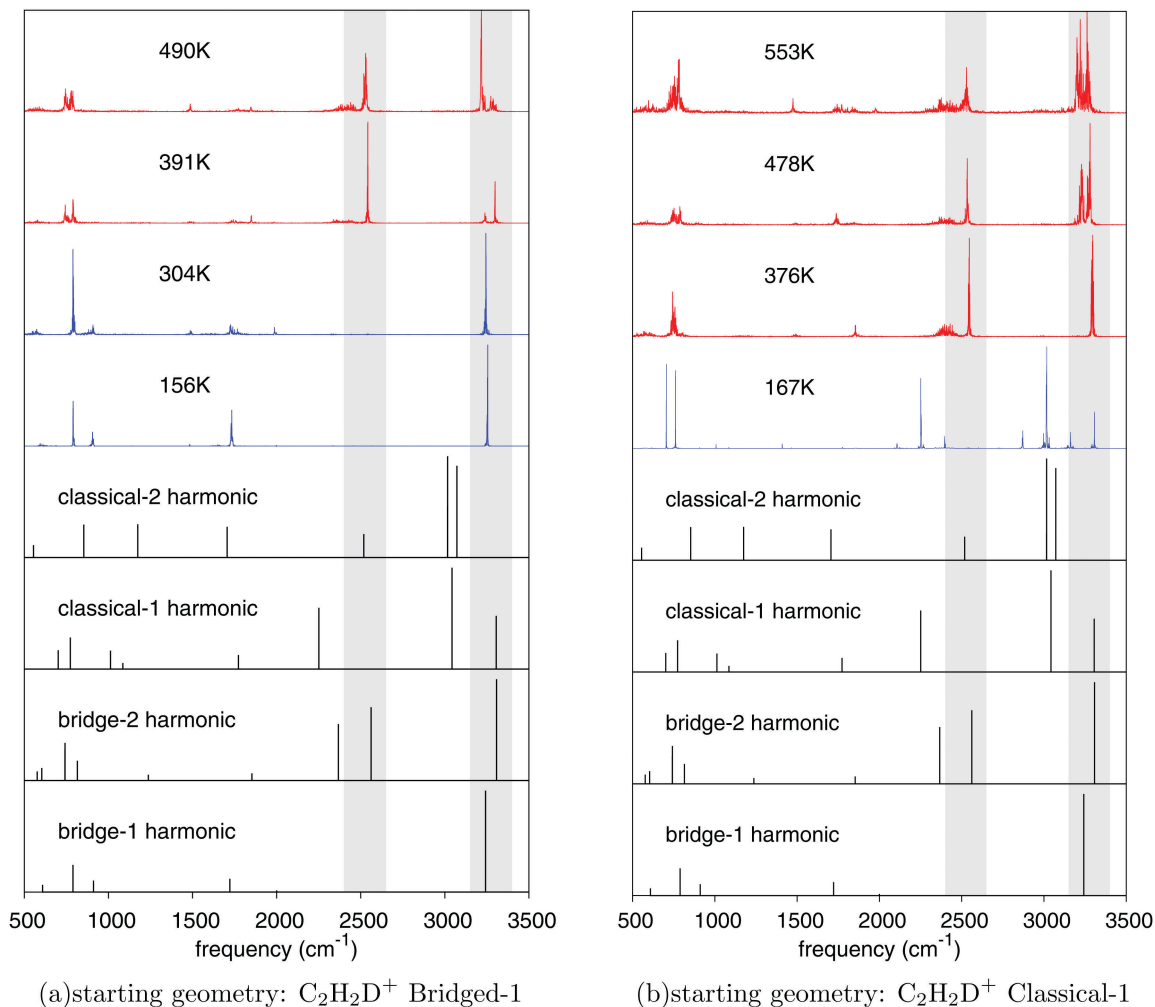
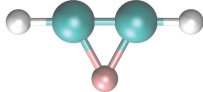
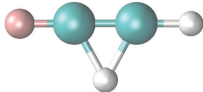
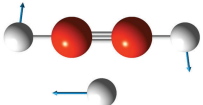
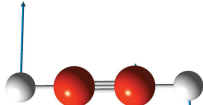
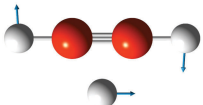

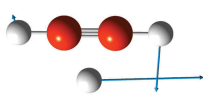
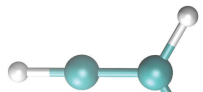
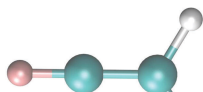
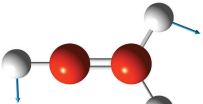
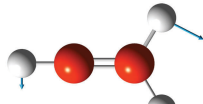
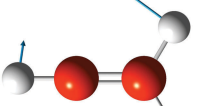
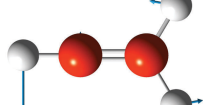


Fig. 10 Calculated IR spectra for the deuterium substituted species $C_2H_2D^+$. In each figure, the bottom four panels are harmonic spectra of the four different isomers shown in Fig. 9. The spectra above are obtained from dynamics trajectories constructed using (a) the Bridged-1 structure as starting geometry and (b) the Classical-1 structure as starting geometry. Trajectories involving dynamical inter-conversion are in red.

Table 3 Harmonic mode descriptions for $C_2H_2D^+$. Only facilitator modes that are directed along the Bridged \leftrightarrow Classical transition paths are shown

					
Frequency (cm^{-1})	IR intensity ^a	Mode description	Frequency (cm^{-1})	IR intensity ^a	Mode description
608.69	30.40		603.93	21.92	
1041.33	0.97		815.50	34.43	
			1237.51	10.00	
					
Frequency (cm^{-1})	IR intensity	Mode description	Frequency (cm^{-1})	IR intensity	Mode description
157.51	28.78		172.90	28.24	
1012.38	47.57		899.18	1.28	

^a In units of $km\ mol^{-1}$.

Classical-2 but not in the starting geometry, Bridged-1. This seems to allude to the fact that the Classical-2 conformation is populated enroute to the Bridged-1 \rightarrow Bridged-2 transformation.

To further probe the transition, we perform time-frequency analysis and the results are shown in Fig. 11 and 12. The results in Fig. 11 clearly show this inter-conversion where the peak at $\approx 2500\ cm^{-1}$ and that at $\approx 3300\ cm^{-1}$ appear alternately, indicating conversion between the Bridged-1 and Bridged-2. In Fig. 12 we present the range of frequencies where the Bridged-1 conformation is mostly dark apart from the single peak at $3291\ cm^{-1}$. As the temperature is increased we populate the $2518\ cm^{-1}$ Classical-2 peak (marked in blue in Fig. 11) and the Bridged-2 peak at $2562\ cm^{-1}$ (marked in red in Fig. 11). This appears to confirm that Classical-2 is populated during the Bridged-1 \rightarrow Bridged-2 transition.

Thus, there are two different pathways for the Bridged-1 \rightarrow Bridged-2 transformation, one wherein the Classical-1 configuration is populated and the other where Classical-2 is populated. In the discussion that follows we differentiate between these pathways using the notation Bridged-1 \rightarrow Classical-1 \rightarrow Bridged-2 and Bridged-1 \rightarrow Classical-2 \rightarrow Bridged-2. This is not a rigorous notation since any intervening appearance of Classical-2 must be followed again by Bridged-1 and Classical-1 before Bridged-2 is populated. We next gauge the probabilities of appearance of the four configurations, and more specifically Classical-1 and Classical-2 structures, during dynamics. Based on the probability of occurrence of these structures (see caption for Fig. 13) we compute the relative stability,

$$\tilde{V}_\beta(R_{B/C}) = \frac{1}{Q} \int dq G(q - R_{B/C}) \exp[-\beta H] V(q), \quad (2)$$

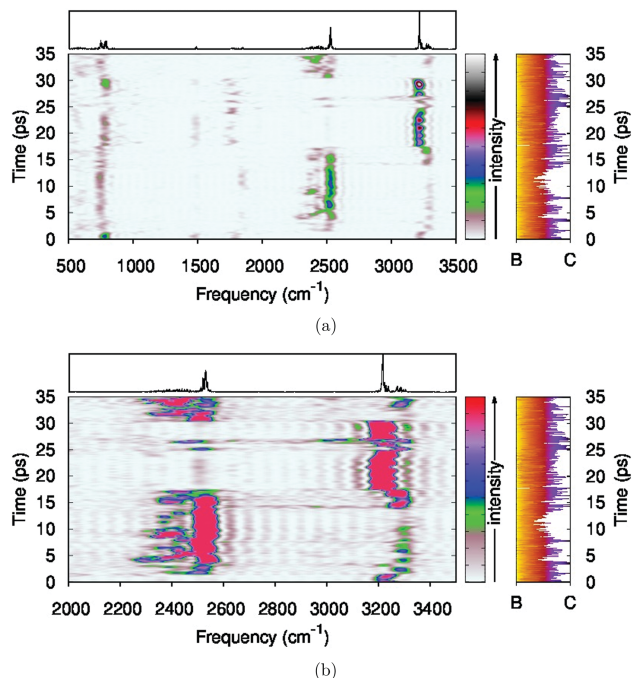


Fig. 11 (a) Two-dimensional time–frequency spectra for $C_2H_2D^+$. Average temperature in this trajectory is 490 K, starting geometry is Bridged-1. (b) Same as (a) but focused to the most relevant region for dynamical inter-conversion. The maximum peak height here is 1/10th the maximum in (a) to assist viewing the appearance of peaks at 3200 cm^{-1} and 2900 cm^{-1} . In all figures, the spectra on the top are corresponding one dimensional $\alpha_{\text{tr}}^{\text{CC}}(\omega)$ -spectra, and the plots on the right side are time evolution of the structure indicator (see Appendix C) where “B” is used to refer to the Bridged structure and “C” for the Classical structure.

$$\exp\left[-\beta V_{\beta}^{\text{PMF}}(R_{\text{B/C}})\right] = \frac{1}{Q} \int dq G(q - R_{\text{B/C}}) \exp[-\beta H] \quad (3)$$

where $G(q - R_{\text{B/C}})$ is a window function that helps compute the localized probability in the vicinity of $R_{\text{B/C}}$ [B/C = Bridged/Classical or any of the other deuterated isomers]. While eqn (2), similar to eqn (1), represents a constrained ensemble averaged potential, eqn (3) defines a potential of mean force, $V_{\beta}^{\text{PMF}}(R_{\text{B/C}})$, acting on the variable $R_{\text{B/C}}$ and is akin to the Helmholtz free energy. In Fig. 13, we present the two potentials defined above for all four singly deuterated configurations. While the average potential values are similar for Bridged-1 and Bridged-2, and similarly for Classical-1 and Classical-2, this is not the case for V_{β}^{PMF} , and the Bridged-2 and Classical-1 are found to be more stable here as compared to their proximal isotopologues. For the Bridged configurations, this is due to the fact that the hydrogen nucleus residing on the exterior location experiences a potential basin that is more shallow as compared to the potential basin on the bridge position, thus supporting more classical micro-states on the terminal position for the heavier deuterium. This is of course a classical interpretation. Quantum-mechanically speaking, the shallow potential around the terminal position leads to a lowering of the deuterium zero-point energy, making deuterium more stable on the terminal position as opposed to on the bridge position. This conclusion is also qualitatively consistent with the simpler harmonic model. Using the most

significant contributions to the zero-point energy under the harmonic approximation ($\approx 3200\text{ cm}^{-1}$ and 2300 cm^{-1}) yields a difference in zero-point energy of $0.75\text{ kcal mol}^{-1}$ where the deuterium is more stable on the terminal location for the bridge configuration. But the harmonic result does not predict the temperature dependence of the stability, which is purely an anharmonic effect as seen in Fig. 13. Thus based on our analysis, the Bridged-2 conformation is more stable relative to Bridged-1.

For the classical isomers, based on our dynamics calculations, the Classical-1 structure is more stable. Using the harmonic analysis for this case, we first note that the relevant proton stretch peaks are at $\approx 3300\text{ cm}^{-1}$ and 3000 cm^{-1} in the bottom panels of Fig. 6. Invoking a simple mass effect on these frequencies yields a difference in zero-point energy of $\approx 0.25\text{ kcal mol}^{-1}$ where Classical-2 is more stable as compared to Classical-1. This is contradictory to what is seen in Fig. 13(b). While these differences are small, and well within the error bars of the electronic structure methods used, the temperature dependence is non-trivial and arises from anharmonic effects. We next discuss the experimental implications of our study.

A. Implications for experiment

Can the “proton shuttle” effect seen here and also alluded to in previous publications^{15,62} be detected by current experiments? In our case the interconversion between the various isomeric forms is noted here through two-dimensional time–frequency analysis, and reemphasized through ensemble populations and associated Helmholtz free-energy calculations in the localized vicinity of the Bridged-1, Bridged-2, Classical-1 and Classical-2 geometries. In essence, as the temperature is increased, the vibrational spectrum changes form and this modification can be understood by reconsidering the vibrational spectrum in terms of the harmonic modes belonging to the constituent isomers that are populated during dynamics. While the desired set of experiments that may probe these results would have both temporal and thermal handles, time–frequency experiments are as yet difficult to perform in the gas-phase.‡ As a result we suggest a careful analysis based on a set of new experiments including (a) low temperature, single photon, argon-tagged action spectroscopy and (b) higher temperature multiple photon dissociation experiments, where the effect of temperature is to populate isomers with canonical weights resulting in spectra that shed light on the relative energetics of the various isomers. This may provide insight into the interconversion process and test the mechanistic hypothesis presented here. There is some precedence to this argument and our rationale towards this suggestion is as follows: in ref. 24, one of us has analyzed the temperature dependent evolution of the vibrational properties of a short-strong hydrogen-bonded system and extracted the complex interplay between vibrational

‡ During preparation of the proofs, it came to the authors’ attention that it could be possible to use circularly polarized light to detect the “Bridged” to “Classical” isomeric transformation. See for example the work of Xuetao Shi, Wen Li and H. Bernhard Schlegel, “Computational simulations of hydrogen circular migration in protonated acetylene induced by circularly polarized light”, *J. Chem. Phys.*, 2016, **145**, 084309.

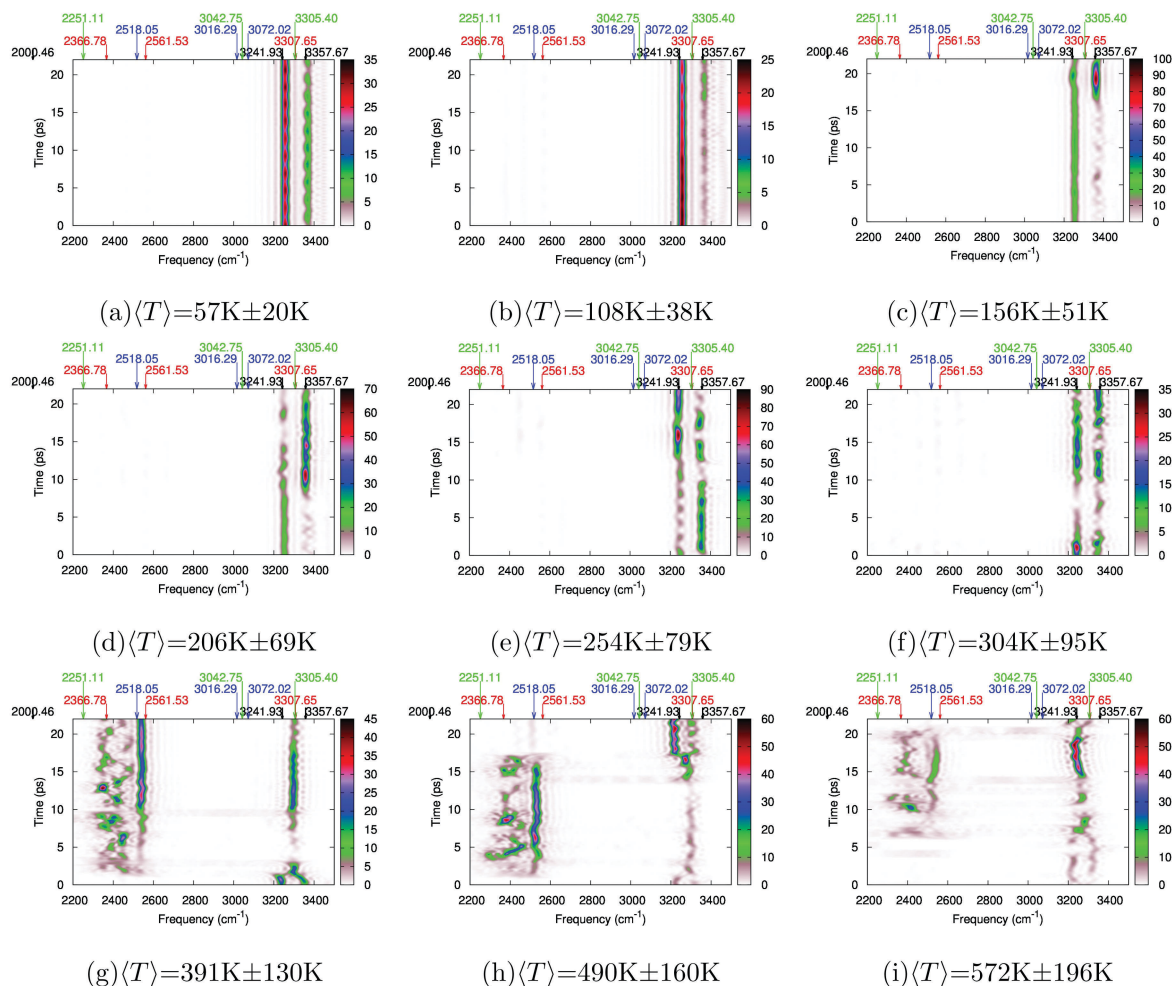


Fig. 12 The quantity $\alpha_v(T, \omega; \Delta T)$ in eqn (B4) is plotted in the time–frequency domain for multiple temperatures. To guide the eye, these figures are also provided as a single animation in the ESI.† The critical Bridged-1 (black), Bridged-2 (red), Classical-2 (blue) and Classical-1 (green) modes are marked.

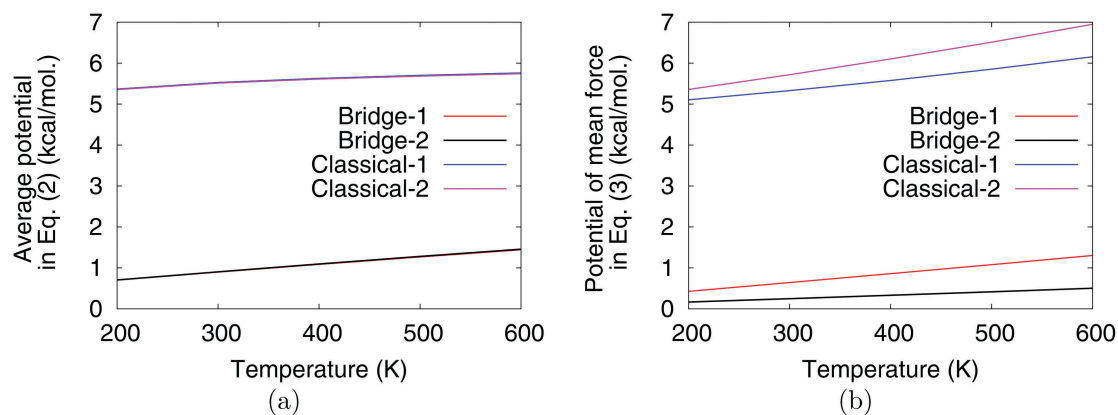


Fig. 13 Average potential, \bar{V}_β in eqn (2) (a), and potential of mean force, V_β^{PMF} in eqn (3) (b), for the four $\text{C}_2\text{H}_2\text{D}^+$ carbocation structures in Fig. 9. While the average potentials for the Bridged and Classical structures are respectively similar, potentials of mean force, being related to the Helmholtz free energy, are different and indicate the Bridged-2 and Classical-1 to be more stable. The quantities are computed from the AIMD trajectories through averages involving 2757715 different structures. Of these, 28.7% (790663 structures) were in Bridged-1, 57.1% (1574718 structures) in Bridged-2, 9.4% (260467 structures) in Classical-1 and 4.8% (131867 structures) in Classical-2.

normal modes that highlight the spectacular differences between the measured IRMPD and argon-tagged action spectroscopy

results for $\text{Me}_2\text{O}-\text{D}-\text{OMe}_2$. This result is summarized through Fig. 14 and reproduced here from ref. 24. In that case, a rich

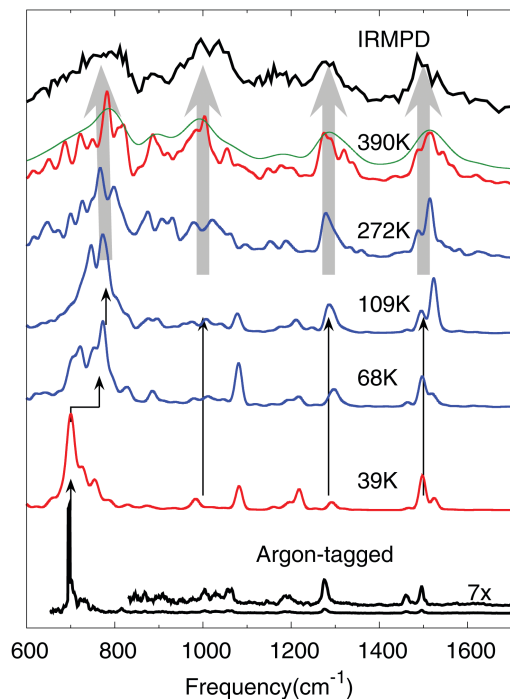


Fig. 14 The progression of finite temperature AIMD spectra for $[\text{Me}_2\text{O}-\text{D}-\text{OMe}_2]^+$ obtained using the $\alpha_{\mu}^{\text{QC}}(\omega)$ intensities of eqn (B2). The 39 K result (red) reproduces the argon-tagged spectrum well whereas the 390 K result (red) reproduces the IRMPD spectrum.²⁴ The AIMD spectra at intermediate temperatures (blue) “interpolate” between the two experimental results. On account of rotational broadening the spectrum filtered using full width at half maximum of about 50 cm^{-1} (green trace) is also shown. This figure facilitates the discussion in Section V(A).

temperature-dependent repartitioning of energy was found within the specific normal modes pertaining to the stretching motion of the intermolecular H/D-bond which greatly affected the observed result. In the current situation, we visualize that differences in the experimental results from argon-tagged action spectroscopy and IRMPD can together shed similar light on the existence and population of the different isomers and associated transition pathways between the multiple Bridged isomers.

VI. Conclusion

We have conducted a detailed investigation on a fundamental carbocation, C_2H_3^+ , that appears to be stabilized by a non-classical chemical bond with the shared proton on a bridge location. This result was noted in previous theoretical studies and more recently in argon-tagged vibrational action spectroscopy experiments. In this publication, we probe this system by analyzing (a) its electronic structure based stability, (b) the effect of the nuclear potential surface that is computed beyond the harmonic approximation by using *ab initio* molecular dynamics, (c) the structural stability arising from nuclear quantum effects probed on reduced dimensional potentials, (d) the fluxional nature of the system using two-dimensional time–frequency vibrational analysis from the *ab initio* molecular dynamics trajectories, and finally (e) the effect of single H/D isotopic substitution.

We find that as the temperature is increased in our simulations, by changing the internal kinetic energy of the system, the hydrogen nucleus at the bridge position circumscribes the carbon–carbon bond by permuting its position with the terminal position hydrogen nuclei. This is very much reminiscent of the Grotthuss mechanism³⁶ from proton transport in aqueous systems. Furthermore, at all temperatures, the classical nuclear distribution function favors the bridge configuration, but quantum mechanically, the reduced dimensional potential surface including bridge and classical positions shows the zero point energy to be above the intervening barrier that separates these two isomeric forms. Despite this, the lower energy hydrogen–nuclear eigenstates are localized on the bridge position.

To break the permutational symmetry of the problem, we have also considered single H/D isotopic substitutions. This leads to four stable isomeric forms where both the Bridged and Classical structures have stable deuteronic positions on two distinct locations. Dynamics allows us to compute the free energetic stability, and here we find that the terminal positions are more favorable for the deuteron for the Bridged isomer, and the doubly terminated carbon position is more stable for the Classical isomer. The result here is also consistently rationalized by gauging the effect of confinement as enforced by the reduced dimensional potentials. However, we also find that isomeric interconversion occurs to a greater extent for the deuterated system. While generally one of the Bridged structures is more stable and dominates the vibrational properties, we find that temperature dependent studies for this system lead to novel results. Finally, we have also suggested experimental implications that may be used to probe the dynamical nature of this problem.

Appendix

A. Reduced dimensional nuclear quantum effects using “distributed approximating functionals” (DAFs)

Quantum nuclear effects were computed by constructing the nuclear Hamiltonian in the coordinate representation, in the dimensionality of R_x (see eqn (1)). Specifically, if R_x is composed of dimensions, $R_x \equiv \{x^1, x^2\}$, with grid discretizations $x^1 \in x_{i_1}^1$ and $x^2 \in x_{i_2}^2$, then

$$H(x_{i_1}^1, x_{i_1'}^1; x_{i_2}^2, x_{i_2'}^2) = - \sum_{I=1}^2 \frac{\hbar^2}{2m} \tilde{K}(x_{i_1}^I, x_{i_1'}^I) + \tilde{V}_{\beta}(x_{i_1}^1, x_{i_1'}^1; x_{i_2}^2, x_{i_2'}^2) \delta_{x_{i_1}^1, x_{i_1'}^1} \delta_{x_{i_2}^2, x_{i_2'}^2}, \quad (\text{A1})$$

for the potential \tilde{V}_{β} in eqn (1). The kinetic energy operator is represented using “distributed approximating functionals” (DAFs):^{23,40–43}

$$\tilde{K}(x_i, x_j) = \frac{1}{\sigma\sqrt{2\pi}} \left(\frac{-1}{\sqrt{2\sigma}}\right)^2 \exp\left(-\frac{(x_i - x_j)^2}{2\sigma^2}\right) \sum_{n=0}^{M/2} \left(\frac{-1}{4}\right)^n \frac{1}{n!} H_{2n+k}\left(\frac{x_i - x_j}{\sqrt{2\sigma}}\right), \quad (\text{A2})$$

where H_{2n+k} are Hermite polynomials. A major advantage of the representation in eqn (A2) is that it provides a banded-Toeplitz representation for the discretized free-propagator and the derivative operator. A Toeplitz matrix is one where $A_{ij} \equiv A(|i - j|)$. Furthermore, the representation in eqn (A2) is banded due to the appearance of the Gaussian function. These properties lead to an $\mathcal{O}(N)$ algorithm for eigenstate calculation and wavepacket propagation as described in the appendix in ref. 63.

B. Velocity and dipole auto-correlation functions to compute spectral intensities and spectral diffusion

The Fourier transform of dipole-dipole auto-correlation is computed here using quantum-nuclear corrections^{64–66} obtained within the Harmonic approximation:

$$\alpha_{\mu}^{\text{QC}}(\omega) \propto \frac{\omega}{1 - \exp(-\beta\hbar\omega)} \times \left\{ \omega [1 - \exp(-\beta\hbar\omega)] \lim_{T \rightarrow \infty} \int_{t=0}^{t=T} dt \exp(-i\omega t) \langle \mu(0) \cdot \mu(t) \rangle \right\}. \quad (\text{B1})$$

The terms inside the curly brackets ($\{\dots\}$) represent the power normalized absorption cross-section.^{67,68} The pre-factor, $\frac{\omega}{1 - \exp(-\beta\hbar\omega)}$, is a quantum-nuclear correction.^{64–66} Over a series of publications^{23,24,33–35,50,69} it has been demonstrated that these correlation functions provide a good estimate of the vibrational spectrum obtained from experimental action spectroscopy. Utilizing the convolution theorem,⁷⁰ eqn (B1) may be rewritten as

$$\alpha_{\mu}^{\text{QC}}(\omega) \propto \omega^2 \lim_{T \rightarrow \infty} \sum_{i=1}^3 \left| \int_{t=0}^{t=T} dt \exp(-i\omega t) \mu_i(t) \right|^2. \quad (\text{B2})$$

For the study of spectral evolution over time, eqn (B2) can be modified to calculate the time–frequency function:

$$\alpha_{\mu}^{\text{QC}}(T, \omega; \Delta T) \propto \omega^2 \sum_{i=1}^3 \left| \int_{t=0}^{t=T} dt \omega(t; T, \Delta T) \exp(-i\omega t) \mu_i(t) \right|^2. \quad (\text{B3})$$

where $\omega(t; T, \Delta T)$ is a window function centered at T with width ΔT . But if the amount of energy in a certain spectral range is to be computed as a function of time, we may utilize a similar expression as that above,⁷¹ by replacing the instantaneous dipoles with instantaneous nuclear velocities, $\mathcal{V}_{ij}(t)$, to obtain

$$\alpha_{\nu}(T, \omega; \Delta T) \propto \sum_{i=1}^{N_{\text{Atoms}}} \sum_{j=1}^3 \left| \int_{t=0}^{t=T} dt \omega(t; T, \Delta T) \exp(-i\omega t) \mathcal{V}_{ij}(t) \right|^2. \quad (\text{B4})$$

In the current study, ΔT is set to 1 ps; the window function is chosen as a step function and smoothing techniques such as those discussed in ref. 71 have not been employed.

C. Reaction coordinate depicting the bridge-terminal transformation

To quantify the proton hopping process, we define the reaction coordinate,¹⁵

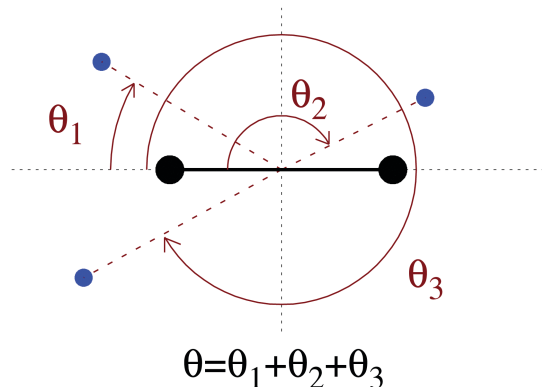


Fig. 15 Angular definitions. Note that θ is used later as a reaction coordinate. Carbon atoms are represented by the large black dots and hydrogen atoms are represented by the small blue dots.

$$\theta = \theta_1 + \theta_2 + \theta_3 \quad (\text{C1})$$

The definition of θ_1 , θ_2 and θ_3 is illustrated in Fig. 15. For the bridged isomer, $|\cos \theta| = 0$ (with $\theta_1 = \pi/2$, $\theta_2 = \pi$, and $\theta_3 = 2\pi$), and for the classical isomer, $|\cos \theta| = 1$ (with $(\theta_1 + \theta_3) = 2\pi$, $\theta_2 = \pi$). Furthermore, $|\cos \theta|$ monotonically changes as the system evolves from bridge to classical and is hence used as the transformation coordinate on the right inset in Fig. 7 and 11.

Acknowledgements

This research is supported by the National Science Foundation grant NSF CHE-1058949 to SSI.

References

- 1 G. K. S. Prakash and P. v. R. Schleyer, *Stable Carbocation Chemistry*, John Wiley And Sons, New York, 1997.
- 2 G. A. Olah and G. K. S. Prakash, *Carbocation Chemistry*, John Wiley And Sons, Hoboken, Nj, 2004.
- 3 J. L. Holmes, C. Aubry and P. M. Mayer, *Assigning Structures To Ions In Mass Spectrometry*, CRC Press, 2006.
- 4 J. M. Greenberg and V. Pirronello, *Chemistry In Space*, Kluwer Academic Publishers, Dordrecht, 1991.
- 5 A. E. Glassgold, A. Omont and M. Guélin, Protonated Acetylene – An Important Circumstellar And Interstellar Ion, *Astrophys. J.*, 1992, **396**, 115.
- 6 B. T. Psciuk, V. A. Benderskii and H. B. Schlegel, Protonated Acetylene Revisited, *Theor. Chem. Acc.*, 2007, **118**, 75.
- 7 C. M. Gabrys, D. Uy, M.-F. Jagod, T. Oka and T. Amano, Infrared Spectroscopy of Carboions. 8. Hollow Cathode Spectroscopy of Protonated Acetylene, C_2H_3^+ , *J. Phys. Chem.*, 1995, **99**, 15611.
- 8 M. Bogey, H. Bolvin, M. Cordonnier, C. Demuyneck, J. L. Destombes, R. Escibano and P. C. Gomez, Tunneling splittings in the rotational spectrum of C_2H_3^+ , *Can. J. Phys.*, 1994, **72**, 967.
- 9 G. E. Douberly, A. M. Ricks, B. W. Ticknor, W. C. McKee, P. v. R. Schleyer and M. A. Duncan, Infrared Photodissociation

- Spectroscopy of Protonated Acetylene and Its Clusters, *J. Phys. Chem. A*, 2008, **112**, 1897.
- 10 M. A. Duncan, Infrared Laser Spectroscopy of Mass-Selected Carbocations, *J. Phys. Chem. A*, 2012, **116**, 11477.
 - 11 E. P. Kanter, Z. Vager, G. Both and D. Zajfman, A measurement of the low energy stereostructure of protonated acetylene, $C_2H_3^+$, *J. Chem. Phys.*, 1986, **85**, 7487.
 - 12 Z. Vager, D. Zajfman, T. Graber and E. P. Kanter, Experimental evidence for anomalous nuclear delocalization in $C_2H_3^+$, *Phys. Rev. Lett.*, 1993, **71**, 4319.
 - 13 D. Marx and M. Parrinello, The Effect Of Quantum And Thermal Fluctuations On The Structure Of The Floppy Molecule $C_2H_3^+$, *Science*, 1996, **271**, 179.
 - 14 L. Knoll, Z. Vager and D. Marx, Experimental Versus Simulated Coulomb-Explosion Images Of Flexible Molecules: Structure Of Protonated Acetylene $C_2H_3^+$, *Phys. Rev. A: At., Mol., Opt. Phys.*, 2003, **67**, 022506.
 - 15 A. R. Sharma, J. Wu, B. J. Braams, S. Carter, R. Schneider, B. Shepler and J. M. Bowman, Potential Energy Surface and MULTIMODE Vibrational Analysis of $C_2H_3^+$, *J. Chem. Phys.*, 2006, **125**, 224306.
 - 16 K. Raghavachari, R. A. Whiteside, J. A. Pople and P. v. R. Schleyer, Molecular orbital theory of the electronic structure of organic molecules. 40. Structures and energies of C1-C3 carbocations including effects of electron correlation, *J. Am. Chem. Soc.*, 1981, **103**, 5649.
 - 17 P. C. Hariharan, W. A. Lathan and J. A. Pople, Molecular orbital theory of simple carbonium ions, *Chem. Phys. Lett.*, 1972, **14**, 385.
 - 18 B. Zurawski, R. Ahlrichs and W. Kutzelnigg, Have the ions $C_2H_3^+$ and $C_2H_5^+$ classical or non-classical structure?, *Chem. Phys. Lett.*, 1973, **21**, 309.
 - 19 J. Weber, M. Yoshimine and A. D. McLean, A CI study of the classical and nonclassical structures of the vinyl cation and their optimum path for rearrangement, *J. Chem. Phys.*, 1976, **64**, 4159.
 - 20 H. Lischka and H. J. Koehler, Structure and stability of the carbocations $C_2H_3^+$ and $C_2H_4X^+$, X = hydrogen, fluorine, chlorine, and methyl. Ab initio investigation including electron correlation and a comparison with MINDO/3 results, *J. Am. Chem. Soc.*, 1978, **100**, 5297.
 - 21 R. C. Fortenberry, X. Huang, T. D. Crawford and T. J. Lee, Quartic Force Field Rovibrational Analysis Of Protonated Acetylene, $C_2H_3^+$, and its Isotopologues, *J. Phys. Chem. A*, 2014, **118**, 7034.
 - 22 J. T. Hougen and L. H. Coudert, Reexamination of the $C_2H_3^+$ microwave and infrared spectra, *J. Mol. Spectrosc.*, 2011, **270**, 123.
 - 23 X. Li, D. T. Moore and S. S. Iyengar, Insights from First Principles Molecular Dynamics Studies Towards Infra-Red Multiple-Photon and Single-Photon Action Spectroscopy: Case Study of the Proton-Bound Di-Methyl Ether Dimer, *J. Chem. Phys.*, 2008, **128**, 184308.
 - 24 X. Li, J. Oomens, J. R. Eyler, D. T. Moore and S. S. Iyengar, Isotope Dependent, Temperature Regulated, Energy Repartitioning in a Low-Barrier, Short-Strong Hydrogen Bonded Cluster, *J. Chem. Phys.*, 2010, **132**, 244301.
 - 25 S. M. Dietrick and S. S. Iyengar, Constructing Periodic Phase Space Orbits from Ab Initio Molecular Dynamics Trajectories to Analyze Vibrational Spectra: Case Study of the Zundel ($H_5O_2^+$) Cation, *J. Chem. Theory Comput.*, 2012, **8**, 4876.
 - 26 N. I. Hammer, E. G. Diken, J. R. Roscioli, M. A. Johnson, E. M. Myshakin, K. D. Jordan, A. B. McCoy, X. Huang, J. M. Bowman and S. Carter, The Vibrational Predissociation Spectra of the $H_5O_2^+RG_n$ (RG = Ar, Ne) clusters: Correlation of the solvent perturbations in the free OH and shared proton transitions of the Zundel ion, *J. Chem. Phys.*, 2005, **122**, 244301.
 - 27 O. Vendrell, F. Gatti and H.-D. Meyer, Dynamics and Infrared Spectroscopy of the Protonated Water Dimer, *Angew. Chem., Int. Ed.*, 2007, **46**, 6918.
 - 28 R. Lindh, B. O. Roos and W. P. Kraemer, A CAS-SCF CI study of the hydrogen migration potential in protonated acetylene, $C_2H_3^+$, *Chem. Phys. Lett.*, 1987, **139**, 407.
 - 29 R. Lindh, J. E. Rice and T. J. Lee, The energy separation between the classical and nonclassical isomers of protonated acetylene. An extensive study in one and n particle space, *J. Chem. Phys.*, 1991, **94**, 8008.
 - 30 J. Li and S. S. Iyengar, Ab initio Molecular Dynamics using Recursive, Spatially Separated, Overlapping Model Subsystems Mixed Within an ONIOM Based Fragmentation Energy Extrapolation Technique, *J. Chem. Theory Comput.*, 2015, **11**, 3978–3991.
 - 31 J. Li, C. Haycraft and S. S. Iyengar, Hybrid extended Lagrangian, post-Hartree-Fock Born-Oppenheimer *ab initio* molecular dynamics using fragment-based electronic structure, *J. Chem. Theory Comput.*, 2016, **12**, 2493.
 - 32 Y. Zhao and D. Truhlar, The M06 suite of density functionals for main group thermochemistry, thermochemical kinetics, noncovalent interactions, excited states, and transition elements: Two new functionals and systematic testing of four M06-class functionals and 12 other functionals, *Theor. Chem. Acc.*, 2006, **120**, 215.
 - 33 S. S. Iyengar, Further Analysis of the Dynamically Averaged Vibrational Spectrum for the “Magic” Protonated 21-Water Cluster, *J. Chem. Phys.*, 2007, **126**, 216101.
 - 34 S. S. Iyengar, M. K. Petersen, C. J. Burnham, V. E. Teige and G. A. Voth, The Properties of Ion-Water Clusters. I. the Protonated 21-Water Cluster, *J. Chem. Phys.*, 2005, **123**, 084309.
 - 35 X. Li, V. E. Teige and S. S. Iyengar, Can the Four-Coordinated, Penta-Valent Oxygen in Hydroxide Water Clusters Be Detected Through Experimental Vibrational Spectroscopy?, *J. Phys. Chem. A*, 2007, **111**, 4815.
 - 36 N. Agmon, The Grotthuss Mechanism, *Chem. Phys. Lett.*, 1995, **244**, 456.
 - 37 Y.-L. S. Tse, A. M. Herring and G. A. Voth, Molecular Dynamics Simulations of Proton Transport in 3M and Nafion Perfluorosulfonic Acid Membranes, *J. Phys. Chem. C*, 2013, **117**, 8079.
 - 38 N. Rega, S. S. Iyengar, G. A. Voth, H. B. Schlegel, T. Vreven and M. J. Frisch, Hybrid Ab-Initio/Empirical Molecular Dynamics: Combining the ONIOM Scheme with the

- Atom-Centered Density Matrix Propagation (ADMP) Approach, *J. Phys. Chem. B*, 2004, **108**, 4210.
- 39 R. Pomes and B. Roux, Theoretical Study of H^+ Translocation Along a Model Proton Wire, *J. Phys. Chem.*, 1996, **100**, 2519.
- 40 S. S. Iyengar and J. Jakowski, Quantum Wavepacket *Ab Initio* Molecular Dynamics: An Approach to Study Quantum Dynamics in Large Systems, *J. Chem. Phys.*, 2005, **122**, 114105.
- 41 J. Jakowski, I. Sumner and S. S. Iyengar, Computational Improvements to Quantum Wavepacket *Ab Initio* Molecular Dynamics Using a Potential-Adapted, Time-Dependent Deterministic Sampling Technique, *J. Chem. Theory Comput.*, 2006, **2**, 1203.
- 42 Y. Huang, D. J. Kouri, M. Arnold, I. T. L. Marchioro and D. K. Hoffman, Distributed Approximating Function Approach to Time-Dependent Wavepacket Propagation in 3-Dimensions: Atom-Surface Scattering, *Comput. Phys. Commun.*, 1994, **80**, 1.
- 43 D. J. Kouri, Y. Huang and D. K. Hoffman, Iterated Real-Time Path Integral Evaluation Using a Distributed Approximating Functional Propagator and Average-Case Complexity Integration, *Phys. Rev. Lett.*, 1995, **75**, 49.
- 44 G. H. Golub and C. F. V. Loan, *Matrix Computations*, The Johns Hopkins University Press, Baltimore, 1996.
- 45 D. C. Sorensen, Implicit Application of Polynomial Filters in a K-Step Arnoldi Method, *SIAM J. Matr. Anal. Apps.*, 1992, **13**, 357.
- 46 J.-W. Shin, N. I. Hammer, E. G. Diken, M. A. Johnson, R. S. Walters, T. D. Jaeger, M. A. Duncan, R. A. Christie and K. D. Jordan, Infrared Signature of Structures Associated with the $H^+(H_2O)_n$ ($N = 6$ to 27) Clusters, *Science*, 2004, **304**, 1137.
- 47 M. Miyazaki, A. Fujii, T. Ebata and N. Mikami, Infrared Spectroscopic Evidence for Protonated Water Clusters Forming Nanoscale Cages, *Science*, 2004, **304**, 1134.
- 48 G. E. Douberly, A. M. Ricks and M. A. Duncan, Infrared Spectroscopy of Perdeuterated Protonated Water Clusters in the Vicinity of the Clathrate Cage, *J. Phys. Chem. A*, 2009, **113**, 8449.
- 49 I. Sumner and S. S. Iyengar, Quantum Wavepacket *Ab Initio* Molecular Dynamics: An Approach for Computing Dynamically Averaged Vibrational Spectra Including Critical Nuclear Quantum Effects, *J. Phys. Chem. A*, 2007, **111**, 10313.
- 50 S. S. Iyengar, Dynamical Effects on Vibrational and Electronic Spectra of Hydroperoxyl Radical Water Clusters, *J. Chem. Phys.*, 2005, **123**, 084310.
- 51 J. J. Valle, J. R. Eyler, J. Oomens, D. T. Moore, A. F. G. van der Meer, G. von Helden, G. Meijer, C. L. Hendrickson, A. G. Marshall and G. T. Blakney, Free Electron Laser-Fourier Transform Ion Cyclotron Resonance Mass Spectrometry Facility for Obtaining Infrared Multiphoton Dissociation Spectra of Gaseous Ions, *Rev. Sci. Instrum.*, 2005, **76**, 023103.
- 52 D. T. Moore, J. Oomens, L. van der Meer, G. von Helden, G. Meijer, J. Valle, A. G. Marshall and J. R. Eyler, Probing the Vibrations of Shared, OH^+O -Bound Protons in the Gas Phase, *ChemPhysChem*, 2004, **5**, 740.
- 53 K. R. Asmis, N. L. Pivonka, G. Santambrogio, M. Brümmer, C. Kaposta, D. M. Neumark and L. Wöste, Gas-Phase Infrared Spectrum of the Protonated Water Dimer, *Science*, 2003, **299**, 1375.
- 54 M. F. Bush, M. W. Forbes, R. A. Jockusch, J. Oomens, N. C. Polfer, R. Saykally and E. Williams, Infrared Spectroscopy of Cationized Lysine and E-N-Methyl Lysine in the Gas Phase: Effects of Alkali Metal Ion Size and Proton Affinity on Zwitterion Stability, *J. Phys. Chem. A*, 2007, **111**, 7753–7760.
- 55 N. L. Pivonka, C. Kaposta, M. Brummer, G. von Helden, G. Meijer, L. Wöste, D. M. Neumark and K. R. Asmis, Probing a Strong Hydrogen Bond with Infrared Spectroscopy: Vibrational Predissociation of $BrHBr^+Ar$, *J. Chem. Phys.*, 2003, **118**, 5275.
- 56 J. R. Roscioli, L. R. McCunn and M. A. Johnson, Quantum Structure of the Intermolecular Proton Bond, *Science*, 2007, **316**, 249.
- 57 J. M. Headrick, E. G. Diken, R. S. Walters, N. I. Hammer, R. A. Christie, J. Cui, E. M. Myshakin, M. A. Duncan, M. A. Johnson and K. Jordan, Spectral Signatures of Hydrated Proton Vibrations in Water Clusters, *Science*, 2005, **308**, 1765.
- 58 G. J. Diebold, F. Engelke, D. M. Lubman, J. C. Whitehead and R. N. Zare, Infrared Multiphoton Dissociation of SF_6 in a Molecular-Beam - Observation of F-Atoms by Chemi-Ionization Detection, *J. Chem. Phys.*, 1977, **67**, 5407.
- 59 E. R. Grant, M. J. Coggiola, Y. T. Lee, P. A. Schulz, A. S. Sudbo and Y. R. Shen, Extent of Energy Randomization in Infrared Multiphoton Dissociation of SF_6 , *Chem. Phys. Lett.*, 1977, **52**, 595.
- 60 D. S. Bomse, R. L. Woodin and J. L. Beauchamp, Molecular Activation with Low-Intensity CW Infrared-Laser Radiation - Multi-Photon Dissociation of Ions Derived from Diethyl-Ether, *J. Am. Chem. Soc.*, 1979, **101**, 5503.
- 61 T. D. Fridgen, L. MacAleese, P. Maitre, T. B. McMahon, P. Boissel and J. Lemaire, Infrared Spectra of Homogeneous and Heterogeneous Proton-Bound Dimers in the Gas Phase, *Phys. Chem. Chem. Phys.*, 2005, **7**, 2747.
- 62 A. V. Burenin, Geometry of the internal dynamics of $C_2H_3^+$ carbocation, *Opt. Spectrosc.*, 2009, **106**, 647.
- 63 A. B. Pacheco and S. S. Iyengar, Multi-Stage *Ab-Initio* Quantum Wavepacket Dynamics for Electronic Structure and Dynamics in Open Systems: Momentum Representation, Coupled Electron Nuclear Dynamics and External Fields, *J. Chem. Phys.*, 2011, **134**, 074107.
- 64 P. H. Berens, S. R. White and K. R. Wilson, Molecular Dynamics and Spectra. II. Diatomic Raman, *J. Chem. Phys.*, 1981, **75**, 515.
- 65 J. S. Bader and B. J. Berne, Quantum and Classical Relaxation Rates from Classical Simulations, *J. Chem. Phys.*, 1994, **100**, 8359.
- 66 C. P. Lawrence, A. Nakayama, N. Makri and J. L. Skinner, Quantum Dynamics in Simple Fluids, *J. Chem. Phys.*, 2004, **120**, 6621.

- 67 R. G. Gordon, Correlation Functions for Molecular Motion, *Adv. Magn. Reson.*, 1968, **3**, 1.
- 68 D. A. McQuarrie, *Statistical Mechanics*, University Science Books, Sausalito, CA, 2000.
- 69 D. Vimal, A. B. Pacheco, S. S. Iyengar and P. S. Stevens, Experimental and Ab Initio Dynamical Investigations of the Kinetics and Intramolecular Energy Transfer Mechanisms for the OH + 1,3-Butadiene Reaction Between 263 and 423 K at Low Pressure, *J. Phys. Chem. A*, 2008, **112**, 7227.
- 70 W. H. Press, S. A. Teukolsky, W. T. Vetterling and B. P. Flannery, *Numerical Recipes in C*, Cambridge University Press, New York, 1992.
- 71 S. M. Dietrick, A. B. Pacheco, P. Phatak, P. S. Stevens and S. S. Iyengar, The Influence of Water on Anharmonicity, Stability and Vibrational Energy Distribution of Hydrogen-Bonded Adducts in Atmospheric Reactions: Case Study of the OH + Isoprene Reaction Intermediate Using *Ab-Initio* Molecular Dynamics, *J. Phys. Chem. A*, 2012, **116**, 399.